Time reversal and imaging for structures

C.G. Panagiotopoulos[1], **Y. Petromichelakis**[1], **C. Tsogka**[1,2]

Abstract

We present a numerical implementation of the time-reversal (TR) process in the framework of structural health monitoring. In this setting, TR can be used for localizing shocks on structures, as well as, for detecting and localizing defects and areas which have suffered damage. In particular, the present study is focused on beam assemblies, typically utilized for simulating structures of civil engineering interest. For that purpose, Timoshenko's beam theory is employed since it is more adequate for describing higher-frequency phenomena. The numerical procedure is explained in detail and the capabilities of the proposed methodology are illustrated with several numerical results.

1 Introduction

Wave propagation in structural components is a topic which appears to be important in numerous cases of engineering interest (Graff, 1975). There are many structures that actually act as, or can be approximated by, assemblings of one-dimensional beam components. In many cases bridges fall in this category, with the typical example being that of truss bridges. We consider here the problem of source shock or defect localization in such structures.

The problem of detection and localization, of defects and areas suffered damage, based on recordings at limited number of spatial points, falls into the category of inverse problems which are usually ill-posed and hard to solve. A computational tool for solving a class of inverse wave (and/or vibration) problems is the time reversal (TR) technique which was originally introduced in (Prada et al., 1995) as a physical process. The principal idea behind TR is to back-propagate the recorded signals but reversed in time. TR consists of two steps: a forward and a backward propagation one. In the forward propagation step, waves are emitted from some source and travel through the medium. During this step the wave-field is being recorded by one or more receivers. In the backward step, the previously recorded signals are reversed in time and they are rebroadcasted from their respective receiver positions. Wave paths that were traversed in the forward propagation step are now reproduced in the backward one Anderson et al. (2008). Ideal conditions for the time reversal process would be those corresponding to the case where receivers fill the whole medium (or its entire boundary), recording the field and its derivatives Fink and Prada (2001), without any noise Givoli (2014). The time *reversibility* is based on the spatial *reciprocity* (symmetry in engineering) and the time reversal *invariance* (under the transformation $t \rightarrow -t$) of linear wave equations. Because of the time-reversibility of the wave equation this procedure leads to a wave that refocuses at the region of the source. A defect or damaged area, can be understood to act as a secondary source and therefore TR can be used for its localization as well. The time reversal technique has been recognized in recent years, because of its robustness and simplicity, as a quite appealing approach with application to numerous disciplines. Interested reader is referred to review articles that exist in the literature with extended presentation of the TR technique and its applications (Yavuz and Teixeira, 2009; Givoli, 2014).

We consider here structures that can be modelled by one-dimensional computational domains such as truss, beam elements, frame structures, etc. For this set-up we develop and test a time reversal procedure that allows for the location of sources, as well as, damaged areas in the structure. Note that in the case of damage our approach relies on the scattered field which is obtained by subtracting the wave-field in the healthy structure from the field in the damaged structure. A migration or back-propagation

[1]Institute of Applied and Computational Mathematics, Foundation for Research and Technology - Hellas, Nikolaou Plastira 100, Vassilika Vouton, GR-700 13 Heraklion, Crete, Greece

[2]Department of Mathematics & Applied Mathematics, University of Crete, Heraklion, Greece, tsogka@uoc.gr

imaging technique that allows for damage localization is also described. It is worth mentioning that our approach, although presented in the one-dimensional setting, it can be easily generalized to two- and three-dimensional domains.

1.1 Longitudinal waves in thin rods

We first consider a simple one-dimensional model that describes propagation of axial waves in a thin homogeneous rod (Graff, 1975). We denote by l, the length of the rod and by A, the cross-section area, which is assumed constant over length. The material properties are described by the elasticity modulus, E, and the mass density, ρ. Let us also denote the longitudinal displacement by $u(x,t)$, the stress field as $\sigma(x,t)$ and the body force as $q(x,t)$.

Assuming linear elastic behaviour and following Hooke's law $\sigma = E\varepsilon$, we obtain the equation of motion,

$$AE\frac{\partial^2 u}{\partial x^2}(x,t) - A\rho\frac{\partial^2 u}{\partial t^2}(x,t) = q(x,t). \tag{1}$$

Here ε is the axial strain defined by $\varepsilon = \frac{\partial u}{\partial x}$. We add to (1) initial,

$$u(x,0) = u_0(x), \qquad \frac{\partial u}{\partial t}(x,0) = \dot{u}_0(x), \tag{2}$$

and bounary conditions

$$u(x,t) = g(t), \quad \forall x \in \Gamma_D, \qquad \frac{\partial u}{\partial x}(x,t) = h(t), \qquad \forall x \in \Gamma_N. \tag{3}$$

Note here that we use the notation Γ_D for the boundary part where displacements, or the generalized degrees of freedom are known. The boundary part Γ_N where spatial derivatives or forces, compatible to the degrees of freedom, are imposed. Finally, we may use Ω for describing the medium itself. In the absence of body forces, that is $q(x,t) = 0$, eq.(1) reduces to the well known wave equation

$$\frac{\partial^2 u}{\partial x^2} = \frac{1}{c_0^2}\frac{\partial^2 u}{\partial t^2}, \tag{4}$$

with $c_0 = \sqrt{\dfrac{E}{\rho}}$, the wave propagationvelocity.

The general solution for eq. (1), under various boundary and initial conditions, as well as, external loading, can be obtained considering an eigenfunction expansion. Alternatively, an integral transformation approach (Laplace, Fourier) or the Green's function method can be followed (Graff, 1975).

Waves incident on the boundary of the domain are reflected in a manner that depends on the nature of the boundary condition as given from eq. (3), or an even more complex (e.g. mixed type) expression. Fixed displacement ($u(x,t) = 0, x \in \Gamma_D$) and free end ($\frac{\partial u}{\partial x}(x,t) = 0, x \in \Gamma_N$) boundary conditions are the two most common cases encountered in applications.

As can be seen in Fig. 1, for the case of fixed end boundary the original pulse changes sign after reflection, while for the case of free end, shown in Fig. 2 the spatial derivative of the original pulse and thus the stress changes sign.

1.2 Flexural waves in thin rods

A more general model that comprises flexural wave propagation can be obtained using the Bernoulli-Euler beam theory. The resulting system of equations is dispersive and allows for infinite wave propagation speed (Graff, 1975) which is certainly unrealistic and contradicts the theory of elastodynamics. Later, Rayleigh solved this problem partially by introducing rotary inertia. We employ here instead

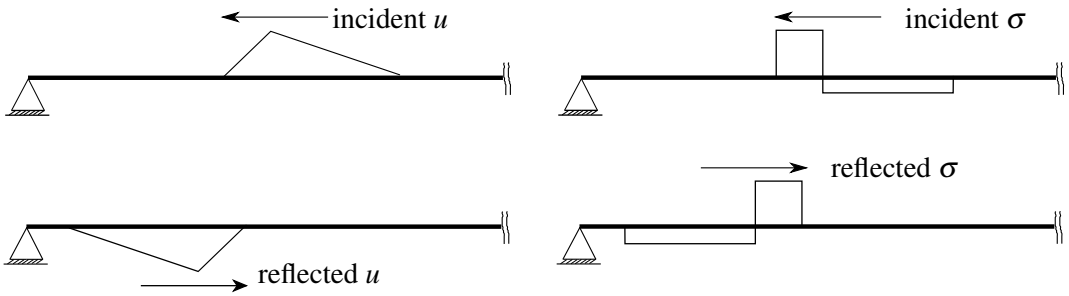

Figure 1: Reflected displacement and stress of incident wave on a fixed end.

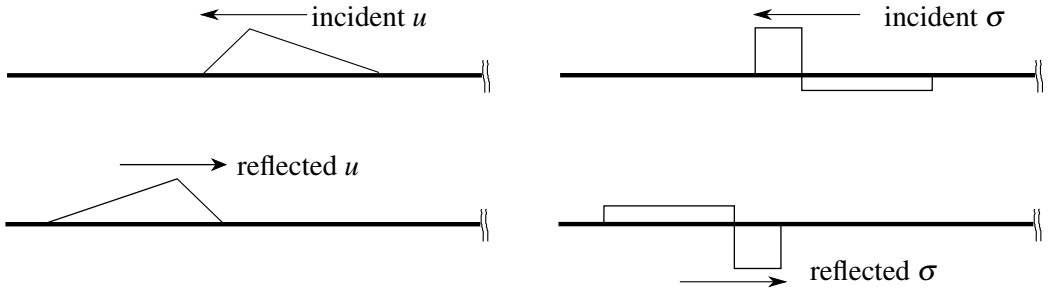

Figure 2: Reflected displacement and stress of incident wave on a free end.

Timoshenko's beam theory (Timoshenko, 1921, 1922) which includes effects of shear and rotary inertia, that are neglected in the previously mentioned Bernoulli-Euler theory. To be more specific, Timoshenko beam incorporates the following two refinements over the Bernoulli-Euler model,

- For both statics and dynamics, plane sections remain plane but not necessarily normal to the deflected midsurface. This assumption allows the averaged shear distortion to be included in both strain and kinetic energy.
- In dynamics, the rotary inertia is included in the kinetic energy,

$$\kappa GA\left(\frac{\partial \psi}{\partial x}-\frac{\partial^2 v}{\partial x^2}\right)+\rho A\frac{\partial^2 v}{\partial t^2}=w(x,t), \tag{5a}$$

$$\kappa GA\left(\frac{\partial v}{\partial x}-\psi\right)+EI\frac{\partial^2 \psi}{\partial x^2}-\rho I\frac{\partial^2 \psi}{\partial t^2}=\mu(x,t). \tag{5b}$$

Here v the transverse displacement and ψ measures the slope of the cross-section due to bending. An additional contribution γ_0 due to shearing effect is included since,

$$\frac{\partial v}{\partial x}=\psi+\gamma_0. \tag{6}$$

External excitation is considered as the prescribed distributed lateral load $w(x,t)$ on the beam and an action of prescribed distributed moments $\mu(x,t)$. Here ρ is the mass density, A is the cross-section area, E is the modulus of elasticity, G is the modulus of rigidity, I is the moment of inertia of the cross-section, and finally κ is a coefficient that depends on the shape of the cross-section (Cowper, 1966). Timoshenko's beam theory assumes two modes of deformation and eq.(5) represents the physical coupling that occurs between them. Wave velocities due to Timoshenko's beam theory are bounded at large wavenumbers having two asymptotic limits, because of the two basic modes of motion (shear and bending) (Fung, 1965), that actually are $c_1^2=\frac{E}{\rho}$ and $c_2^2=\frac{\kappa G}{\rho}$.

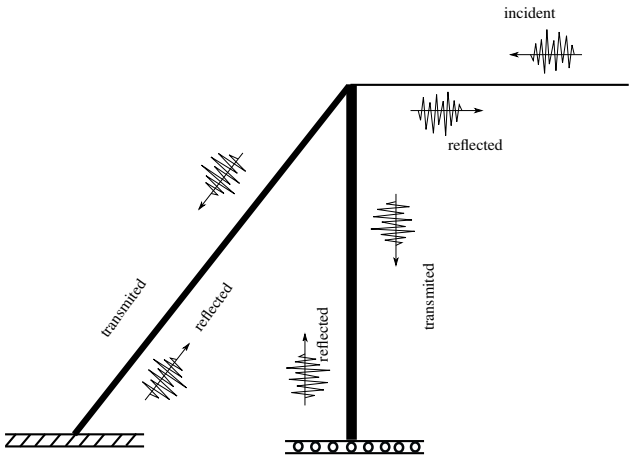

Figure 3: A junction of three coupled beams (1D elastic domains), of different characteristics (cross-section, material), with corresponding propagating waves.

1.3 Assembly of structural members

The most convenient way to introduce more complicated structures, consisting of a collection of arbitrarily oriented one-dimensional components, is by matrix representation. A suitable approach is the finite element method (FEM), for which stiffness and mass matrix for axial deformation, as well as, for transverse displacement and slope according to Timoshenko beam, are available (Przemieniecki, 1968). This is illustrated in Fig. 3, where a junction of three distinct one-dimensional domains that meet each other, is shown. Each of the structural components, is assumed to be capable of bearing axial as well as bending loading. Axial and transverse-rotational modes are uncoupled, as has been explained earlier (5), on the local reference coordinate system. However, on the global reference coordinate system ,and because of the interaction at the junctions of the assembly, coupling takes place. At the junction, equilibrium of forces and continuity of displacements is forced, while additional boundary conditions might be considered depending on the characteristics of the problem. Special techniques for taking into account general non-homogeneous time-dependent boundary conditions in the context of FEM have been developed in (Panagiotopoulos et al., 2011; Paraskevopoulos et al., 2010).

On junctions where two rods, as shown in Fig. 3, of different properties (i.e., cross-section, mass density or elasticity modulus), join together, we impose the balance of force and continuity of the kinematic field (displacement, velocity). We mention here that while wave equation for a rod predicts no distortion in the propagated wave, dispersive effects in rods may arise, when considering discontinuous cross sections.

2 Numerical implementation

Several numerical methods have been developed for computing the solution of wave propagation problems in structures. We just namely mention Galerkin FEM (Le Guennec and Savin, 2011), Spectral Element Method (Doyle, 1989; Gopalakrishnan et al., 2008), as well as, other mixed formulations of FEM (Bécache et al., 2002). Here we have adopted conventional FEM, first because engineering community is much more familiar to that and also because of its versatility regarding spatial and time discretization (Cook et al., 2001).

More specifically in our numerics we use stiffness and mass matrices for Timoshenko beam as given in (Przemieniecki, 1968), together with the familiar Newmark time integration algorithm (Bathe, 2006) while other energy conserving algorithms (Simo and Tarnow, 1992) have also been tested.

As it will be made clear later, a crucial quantity in our framework is the rate of mechanical energy.

That energy for an one dimensional domain, in which we have axial and transverse deformation, as well as, rotation is given by,

$$\mathscr{E}(t) = \underbrace{\frac{1}{2}\int_0^L \rho A\left(\frac{\partial u}{\partial t}\right)^2 + \rho A\left(\frac{\partial v}{\partial t}\right)^2 + \rho I\left(\frac{\partial \psi}{\partial t}\right)^2 dx}_{\text{kinetic energy}}$$

$$+ \underbrace{\frac{1}{2}\int_0^L EA\left(\frac{\partial u}{\partial x}\right)^2 + \kappa GA\left(\frac{\partial v}{\partial x} - \psi\right)^2 + EI\left(\frac{\partial \psi}{\partial x}\right)^2 dx}_{\text{potential elastic energy}} \quad . \tag{7}$$

We will further refer to the one half of the integrand quantity as the density of the total energy rate, denoted by $e(x,t)$.

2.1 Discretized equations of motion

After spatial discretization using the FEM, system of equations (1) and (5) may be written in an algebraic (matrix) form as

$$\mathbf{M}\ddot{\mathbf{u}} + \mathbf{K}\mathbf{u} = \mathbf{f}, \tag{8}$$

where $\mathbf{M}$ and $\mathbf{K}$ are the mass and stiffness $N \times N$ matrices, $\mathbf{u}$ is the $N \times 1$ vector of unknown degrees of freedom (dofs) of the system (axial and transverse displacements (u,v) as well as the slope ψ) while dotted variables denote derivatives with respect to time. Furthermore, $\mathbf{f}$ is the $N \times 1$ vector of external loading. Up to now we have not considered any damping, however all structural systems involve some damping and for this case the respective system of equations would be,

$$\mathbf{M}\ddot{\mathbf{u}} + \mathbf{C}\dot{\mathbf{u}} + \mathbf{K}\mathbf{u} = \mathbf{f}, \tag{9}$$

with $\mathbf{C}$ a damping matrix. Accurate assumption on damping of a structural system is not always an easy task, however a common hypothesis is that of Rayleigh's damping (Clough and Penzien, 1993) given as $\mathbf{C} = a_m\mathbf{M} + a_k\mathbf{K}$.

Equations (8) and (9) are known as the semi-discrete equations of motion since they are only discretized with respect to the spatial variables (and not the time). In principle, any standard procedure for the solution of differential equations with constant coefficients, could serve in order to deal with these systems of equations. However, it is more convenient to use a direct integration method, where equation (8) (or (9)) are integrated using a numerical step-by-step procedure. Two are the main components of such direct integration techniques, first, instead of trying to satisfy (9) at any time t, it is aimed to be satisfied only at discrete times Δt apart. The second idea is that a variation of the kinematic field, within each time interval Δt, is assumed. For an extensive presentation the interested reader is referred to (Belytschko and Hughes, 2014).

For linear systems such as (8) and (9), where the principle of superposition holds, the solution can be obtained by Fourier transform (frequency domain) procedures, as well as, by applying convolution integral (time domain) methods. In what follows, in subsections 2.2 and 2.3, we mainly reproduce well known material found in the literature (Clough and Penzien, 1993). In subsequent sections, 3 and 4, we clarify the reason for which we need such an approach. In such a case, one would need the unit-impulse transfer functions that actually are the Green's function analogue for the discretized systems. Here we numerically obtain these functions by utilizing the FEM. A thorough study on the relation of Green's functions and FEM for the case of quasi-static conditions may be found in recent literature (Hartmann, 2013).

2.2 Time domain formulation

Assuming that the system is subjected to a unit-impulse loading in the j^{th} dof, while no other loads are applied, the force vector $\mathbf{f}(t)$ consists only of zero components except for the j^{th} term which is expressed by $f_j(t)=\delta(t)$. Solving (8) for this specific loading, the i^{th} component in the resulting displacement vector will then be the free-vibration response in that dof caused by a unit-impulse in coordinate j. Therefore by definition this i^{th} component motion is a unit-impulse transfer function, which will be denoted herein by $h_{ij}(t)$.

If the corresponding loading in the j^{th} dof was a general time varying load $f_j(t)$ rather than a unit-impulse loading, the dynamic response for the i^{th} dof could be obtained by superposing the effects of a succession of impulses in the manner of the Duhamel's integral, assuming zero initial conditions. The generalized expression for the response of the i^{th} dof to the load at j is the convolution integral, as follows:

$$u_{ij}(t) = \int_0^t f_j(\tau) h_{ij}(t-\tau)\, d\tau, \qquad i = 1,2,\ldots,N \tag{10}$$

and the total response for the i^{th} dof produced by a general loading involving all components of the load vector $f(t)$ is obtained by summing the contributions from all load components:

$$u_i(t) = \sum_{j=1}^{N} \left[\int_0^t f_j(\tau) h_{ij}(t-\tau)\, d\tau \right], \qquad i = 1,2,\ldots,N. \tag{11}$$

2.3 Frequency domain formulation

The frequency-domain analysis is similar to the time-domain procedure in that it involves superposition of the effects for dof i of a unit load applied to the dof j, however, in this case both the load and the response are harmonic. Hence, the load has the form $f_j(t)=\exp i\omega t$, while the corresponding steady-state response for i^{th} dof will be $\widehat{h}_{ij}(\omega)\exp(i\omega t)$ in which $\widehat{h}_{ij}(\omega)$ is defined as the complex frequency response transfer function.

If the loading corresponding to j^{th} dof was a general time varying load $f_j(t)$ rather than time-harmonic, the forced vibration response of the i^{th} dof could be obtained by superposing the effects of all the harmonics contained in $f_j(t)$. For this purpose the time domain expression of the loading is Fourier transformed to obtain

$$\widehat{f}_j(\omega) = \int_{-\infty}^{\infty} f_j(t) \exp(-i\omega t)\, dt \tag{12}$$

and then by inverse Fourier transformation the responses to all of these harmonics are combined to obtain the total forced vibration response for the i^{th} dof, as follows (assuming zero initial condittions):

$$u_{ij}(t) = \frac{1}{2\pi} \int_{-\infty}^{\infty} \widehat{h}_{ij}(\omega) \widehat{f}_j(\omega) \exp(i\omega t)\, d\omega. \tag{13}$$

Finally, the total response for i^{th} dof produced by a general loading involving all components of the load vector $\mathbf{f}$ could be obtained by superposing the contributions from all the load components:

$$u_i(t) = \frac{1}{2\pi} \sum_{j=1}^{N} \left[\int_{-\infty}^{\infty} \widehat{h}_{ij}(\omega) \widehat{f}_j(\omega) \exp(i\omega t)\, d\omega \right], \qquad i = 1,2,\ldots,N. \tag{14}$$

Equations (11) and (14) constitute general solutions to the coupled equations of motion, assuming zero initial conditions. Their successful implementation depends on being able to generate the transfer functions $h_{ij}(t)$ and $\widehat{h}_{ij}(\omega)$ efficiently. While this is not practical for the time-domain functions, efficient procedures for implementing the frequency-domain formulation can be developed.

Moreover, it can also be shown that any unit impulse response transfer function $h_{ij}(t)$ and the corresponding complex frequency response transfer function $\widehat{h}_{ij}(\omega)$ are Fourier transform pairs, provided some damping is present in the system in order for the inverse trasnformation of eq. (13) to exist.

3 Time reversal process

Assuming a medium Ω under given boundary and initial conditions, let a sub-domain of it Ω_s, where excitation is applied and a second one Ω_r, where sensors record response in time, intersection $\Omega_s \cap \Omega_r$ might be non-empty. Medium Ω might be heterogeneous, embedding a number of scatterers, and may be of complicated geometry.

According to the time reversal concept (Fink et al., 2000), an input signal can be reconstructed at an excitation point $x_s \in \Omega_s$ if an output signal recorded at a collection of points $x_r \in \Omega_r$ is re-emitted in the same medium after being reversed in the time domain. This process is referred to as time reversal and is based on the spatial *reciprocity* (also found as symmetry in engineering) and the time reversal *invariance* (under the transformation $t \rightarrow -t$) of linear wave equations. A review article on time reversal and its applications has been recently published (Givoli, 2014), while a brief presentation and applications on structural systems may be found in (Kohler et al., 2009). Our methodology is also described in (Tsogka et al., 2015; Panagiotopoulos et al., 2015) while a different implementation for one-dimensional domains is considered in (Guennec et al., 2013) using a transport equation model for the energy.

While TR was originally developed for undamped systems, it is believed and has been shown, that it may also be applied to systems with damping (Ammari et al., 2013). Solving (8) or (9) for the unit impulse force vector, corresponding to the source dof, we compute the solution at all dofs while keeping track of the dofs corresponding to x_r. That is the forward propagation of the procedure. By reversing the response at x_r in time and considering it as the new excitation imposed on the corresponding dofs, we define the backward step of the procedure. Time reversal refocusing states that the solution will refocus at the original source location at time $t = 0$.

Furthermore, considering defects as points of secondary sources we may define a methodology for defect or damage identification and localization in structures. In what follows we present some elementary results considering the above framework.

3.1 Instrumentation and data collection

In this work we describe the numerical implementation of time reversal in elastic media and carry out simulations in order to assess the effectiveness of this process in damage identification problems of structures. We assume that the medium Ω is one-dimensional or an assembly of one dimensional components. Response might be recorded on N_r sensors, belonging in $\Omega_r \in \Omega$, while excitation is assumed to be produced by N_s source points forming $\Omega_s \in \Omega$, where Ω the collection of the entire set of dofs that describe and represent the problem. These two subsets, Ω_r and Ω_s may be totally separated, coincide or just have an overlap.

In structural health monitoring (SHM) the forward step of TR corresponds to a physical process where the data response matrix is collected on a set of sensors located on the structure and being compatible with dofs $\boldsymbol{u}_r$, $r = 1, \ldots, N_r$.

Remark that at a specific location in space, we have in general associated more than one dofs corresponding to the number of unknowns at this location. Therefore each column of the response matrix corresponds to the response received at all sensors and in all dofs, $\boldsymbol{u}_r$, when a source point emits a pulse from a location compatible with a specific dof, $\boldsymbol{u}_s$. In our case, the forward step is numerically simulated. A source located on the structure emits a pulse compatible with a specific dof, $\boldsymbol{u}_s$, and the

response is recorded at the receiver locations and corresponding dofs $\boldsymbol{u}_r$. Considering that these pulses emulate impulses, the matrix constructed by this process is an approximation of the impulse response matrix (IRM) with components the $h_{ij}(t)$ given in eq. (10) for $i = 1,\ldots,N_r$ and $j = 1,\ldots,N_s$. In the case where we try to identify and locate defects or damages in the structure, we may sometimes work with the "scattered" IRM which will contain the difference of the impulse response of the damaged minus the impulse response of the healthy configuration of the structure.

3.2 Source localization

Consider a rectangular beam of finite length L=30m and square cross section of unit area, an elastic material of modulus E=1Pa, Poisson's ratio ν=0.25 and mass density ρ=1kg/m^3, with both ends fixed (Dirichlet homogeneous boundary conditions). Wave propagation velocities are c_0=c_1=1m/s, while c_2=0.578m/s, considering κ=5/6. For the simulation we use a mesh of 1200 elements that means a size h=0.025m and a time step dt=0.025s. We assume a source located at x_s=0.75L having both axial and transverse components corresponding to u and v, and being a Ricker wavelet in time, given by:

$$f(x,t) = a\delta(x-x_s)\left(1-2\pi^2 s^2 (t-t_0)^2\right)e^{-\pi^2 s^2 (t-t_0)^2},$$

with t_0=3s and s=1.5, and the amplitude a=1000. We also assume a sensor located at the central point x_r=0.5L recording the full kinematic field, that is, the group of dofs u, v and ψ in time. The total time of the experiment is T=t_0+$2L/c_1$=63s. Numerically resolving the problem we compute the response's time history. Wave propagation on the length of the rod is depicted in Figs. 4, 5 and 6, 7. Furthermore, Fig. 8 shows the response in time as recorded on sensor at x_r for the full set of dofs. This latter response is then reversed in time and imposed as loading on x_r to solve the backward step. It is expected, and also confirmed by results in plots of Fig. 9, the refocusing of the wave at the original source point x_s for time $T-t_0$=60s.

The quality of the refocusing can be improved by increasing the number of recording sensors as illustrated in the same Fig. 9 where ten and one hundred sensors, equally spaced on the length, have also been used. A clear improvement is obtained and we observe a decrease in the amplitude of the ghosts that are due to reflections of the propagating waves on the boundaries as the number of sensors increases. A quantitative analysis of the improvement in the case of acoustic waves was carried out in (Tsogka et al., 2015) where we show that the signal to noise ratio (SNR), defined as the value at the source divided by the maximal ghost value, is linear with respect to the number of receivers.

3.3 Damage identification

We assume here a damaged area on the rod taking place from x_1=9.025m to x_2=9.125m where the material has reduced modulus E_d =0.1Pa corresponding to a velocity $c_{0,d}$ =0.316m/s. In the forward step source and receivers points, as well as, the Ricker pulse emitted, kept the same as for the previous example. We are now interested in the scattered field because of the damaged area, that is computed as the difference of the wave propagating in the damaged configuration minus the corresponding in the original reference state; The axial component motion of that scattered field is depicted in Fig. 10, where it can be observed that letting the pulse emitted from the source at x_s=22.5m on the initial time t_0=3s, the wave travelling with velocity c_0=1m/s, arrives at x_1=9.125m at a time of about 16s. This is the approximate time that the scattered field starts to appear. It is obvious that in this case this secondary source is of more complicated form than that of the original source shown previously, for example, in Fig. 5. However it is possible by using this scattered wave field and the time reversal procedure, that is, reverse in time the "recorded" scattered field and re-emit it, to construct images of the damage shown in plots of Fig. 11. As it can also be seen in these plots, we use axial and transverse components to make images and locate damage, indicated by peak response, using different times, 46.3 and 37.5s respectively, due to the fact that these two waves travel with different velocities as has been stated previously in this chapter. What else can be seen in these plots, is that by increasing the number of receiver points images

are improved and the results appear to have an increased SNR. Finally, let us note that some peaks of noise that do not seem to decrease, are due to source rather than receivers and we would rather need to increase the number of source points in order to further improve the quality of image (Tsogka et al., 2015).

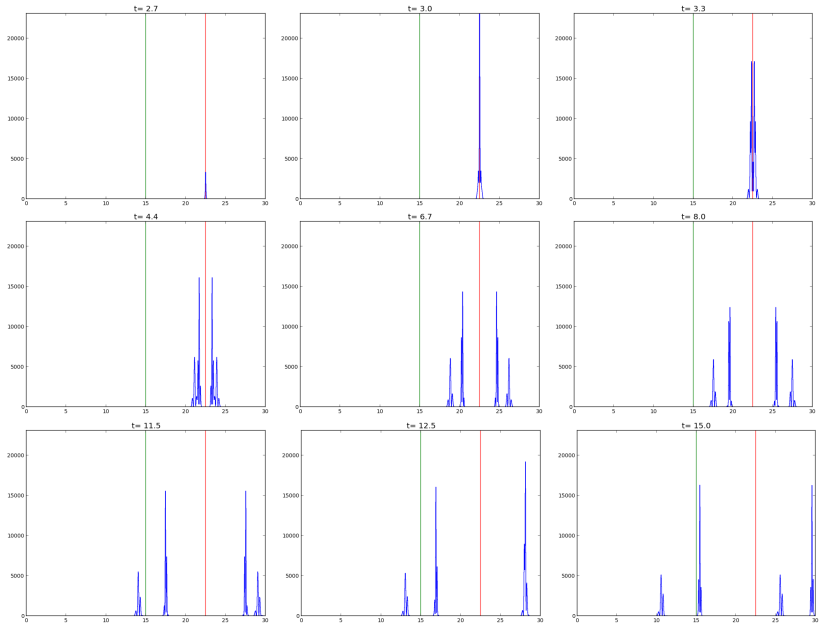

Figure 4: Forward wave propagation for the rate of the total energy, the red vertical line shows the location of the source while the green the location of the sensor.

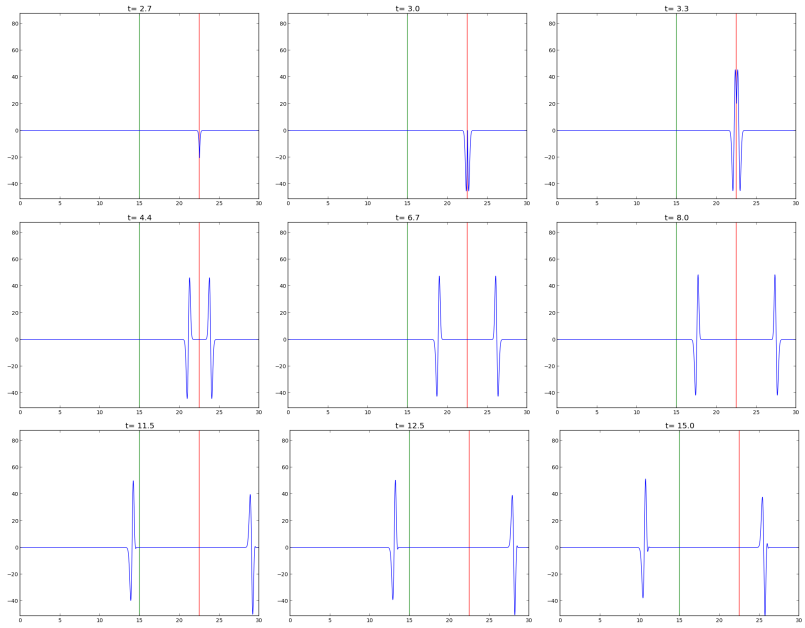

Figure 5: Forward wave propagation for the axial displacement u, the red vertical line shows the location of the source while the green the location of the sensor.

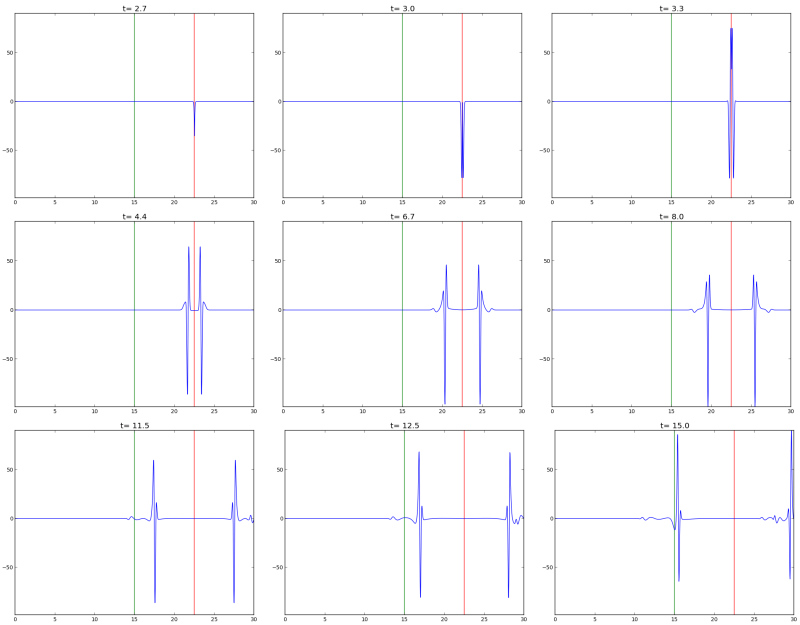

Figure 6: Forward wave propagation for the transverse displacement v, the red vertical line shows the location of the source while the green the location of the sensor.

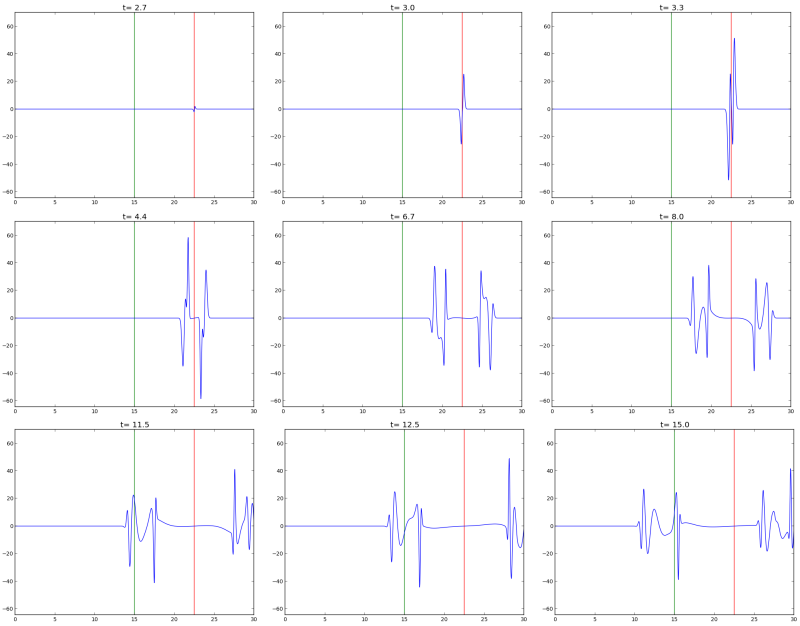

Figure 7: Forward wave propagation for the slope ψ, the red vertical line shows the location of the source while the green the location of the sensor.

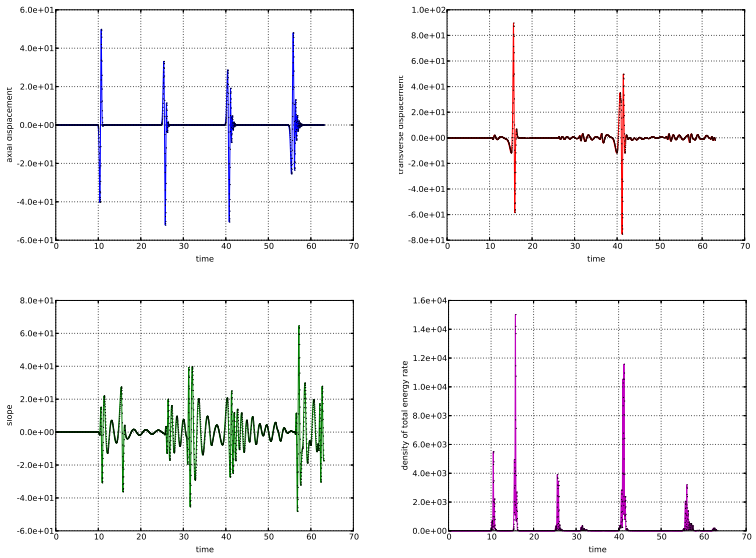

Figure 8: Response recorded on a sensor at x_r for axial, vertical displacements u, v and slope ψ. Furthermore, the density of the total energy rate e on the same sensor is plotted.

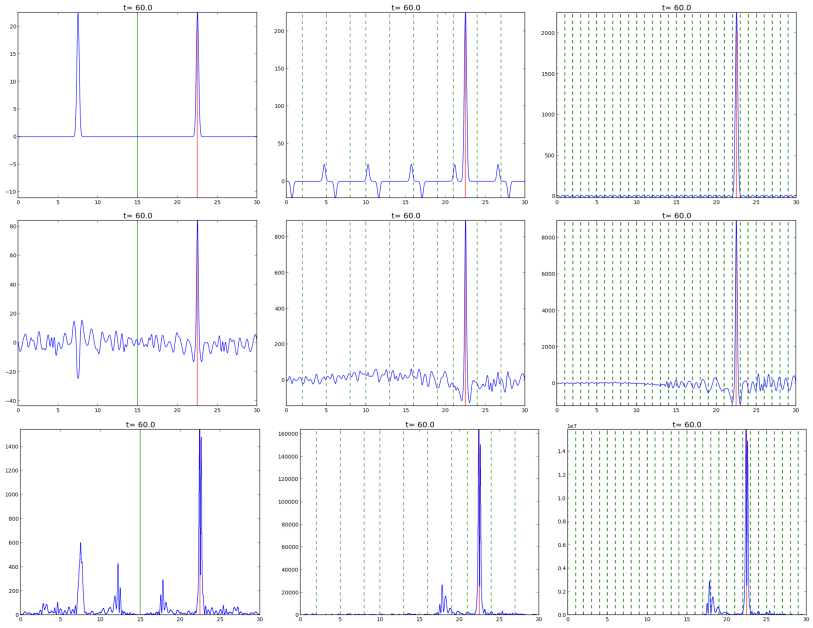

Figure 9: Source refocusing after backward imposition of time reversed data. From upper to lower corresponds to u, v and rate of total energy density h, while from left to right number of receivers corresponds to 1,10 and 100, respectively.

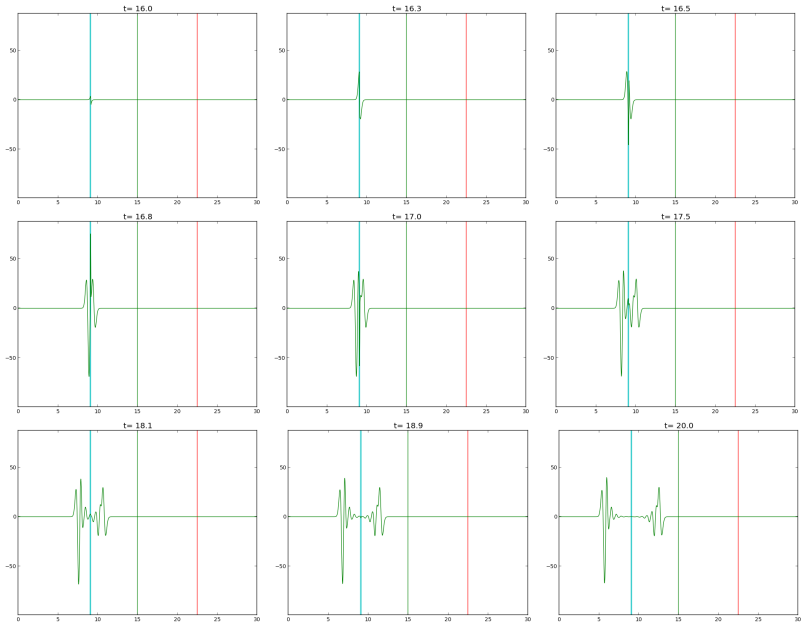

Figure 10: Forward scattered wave propagation for the axial displacement u, the red vertical line shows the location of the source while the green the location of the sensor.

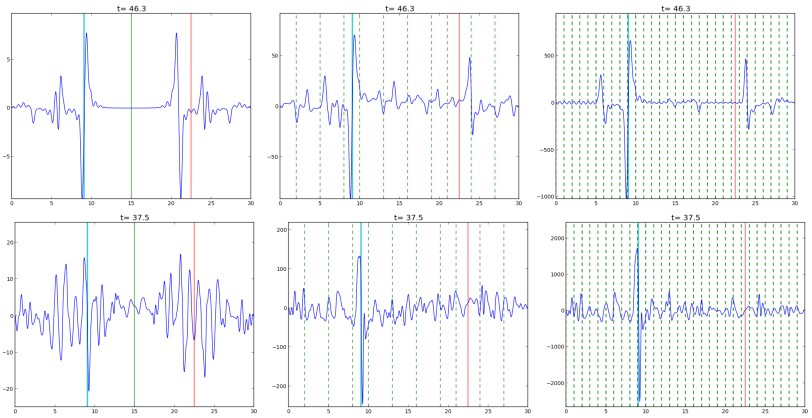

Figure 11: Damage refocusing after backward imposition of time reversed data. Upper raw imaging by using data for the axial displacement, while lower for the transverse displacement. Damage area is pointed by two vertical cyan lines. One receiver is used for the left column figures while ten receivers are used to produce the medium and one hundred for the rightmost images. For the axial displacement improvement in the localisation is observed by increasing the number of receivers while a persistent ghost remains when the transverse displacement is used.

3.4 A bridge-like structural example

In this quite academic example, a bridge like frame structure is considered. Assumptions for the Timoshenko beam have been once again assumed while a modified material for both the original, as well as, the damaged configurations, has been considered. The difference, with respect to the material used

before, is the mass density which in this case is ρ=0.1kg/m^3 and the corresponding wave propagation velocities are c_0=c_1=3.46m/s, while c_2=2.0m/s. Once again unit cross-sections are assumed. The total maximum length of the structure is L=40m and its height h=5m while it consists of eight spans of equal length. We present only the case of damage identification, however, numerical experiments for source localization have also concluded perfect results. As regards boundary conditions we considered restrained both horizontal and vertical displacement of the furthest right and left ends of the structure. Numerical solution presented in this example is for a total number of 1560 elements of lengths 0.0833m (vertical elements), 0.095m (horizontal elements) and 0.1265m (inclined elements). The total time considered is t=26.3875s while a time step dt=0.0125s has been chosen, that results a total number of 2111 time steps. Originally, it is assumed that possible positions for the sensor's placements are the junctions indicated in Fig. 12 as s_i, where $i \in [1,14]$, and also it is possiblle for any of the three dofs to be recorded and then re-emitted. The source node, where a Ricker wavelet has been imposed, coincides with point of s_3. In Fig. 13 the response, numerically obtained and recorded, on sensor s_{14} for both the reference and damaged configurations, together with their difference which results the scattered field, is plotted. The scatterd field is actually the one that is reversed in time and re-emitted. Similar data are plotted for the central point of the damaged zone in Fig. 14.

We present here results for three alternative sensors' distirbutions, while we consider as recorded and re-emitted responses these of the two translational dofs. According to the first configuration we assume as active sensors these of s_7 and s_9, while for the second one these of s_2, s_7, s_9 and s_{12} and the final one where we assume active sensors on the whole set of possible sensors. We have also kept track for both the Euclidian norm and the energy density as possible variables to construct the image. The time evolution of these quantities are shown in the plots of Fig. 15. The maximum value for the Euclidian norm (left) appears at time t=13.0125s which corresponds to discrete time step i_{nrm}=1041, while for the energy rate (right) at time t=17.0375s which corresponds to the discrete time step i_{nrg}=1363. In order to construct an image using the energy norm, shown in Fig. 17, we use the i_{nrg} time step for all the three sensor configurations, while by using the Euclidian norm, shown in Fig. 16, both the i_{nrm} and i_{nrg} steps are used just for the case of configuration where the whole set of sensors are considered. We may also observe the fact that the reversed time t=26.3875−17.0375=9.35s approximately corresponds to the time that the scattered signal starts to be emitted at the location of the damage as a secondary source, which might be seen also in Fig. 14. As it can be observed in the plots of figures 16 and 17, the energy density appeared to be a more suitable variable for imaging in this case, since location of damage has been found very accurately. It is also observed in the case of Fig. 16, that improvement of imaging is achieved with increased number of sensors that record and re-emit the response.

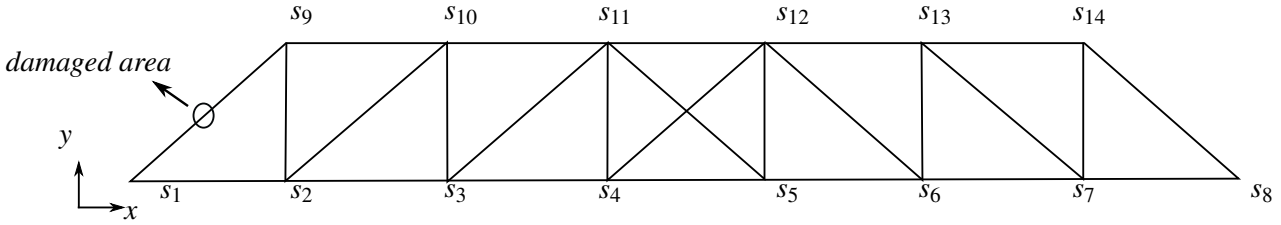

Figure 12: A sketch of the bridge structure where the position of damage is depicted and also points of possible sensor placement are indicated.

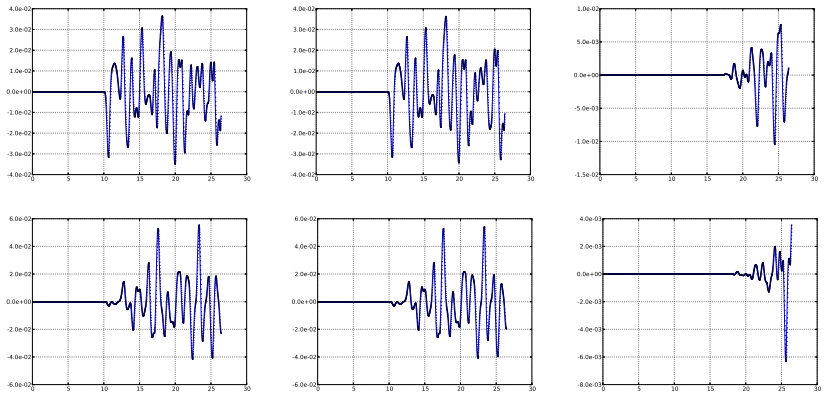

Figure 13: Horizontal (upper row) and vertical (lower row) displacements recorded on sensor s_{14} during the forward process. From left to right is depicted the response on healthy (reference) structure, damaged and their difference which is the scattered field.

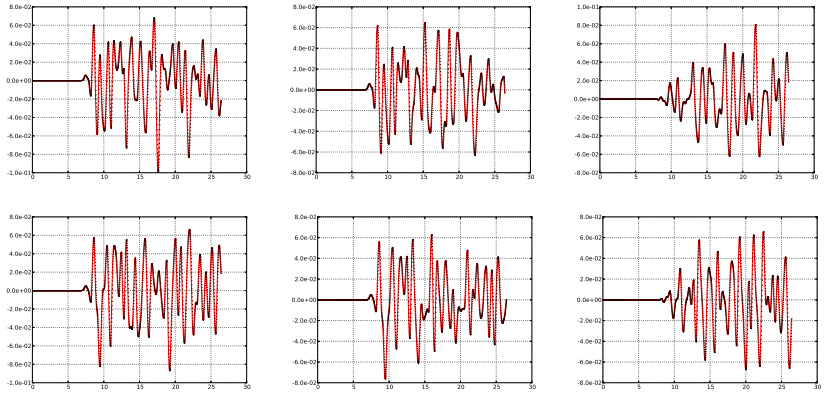

Figure 14: Horizontal (upper row) and vertical (lower row) displacements' response on the damaged zone during the forward process. From left to right is depicted the response on healthy (reference) structure, damaged and their difference which is the scattered field.

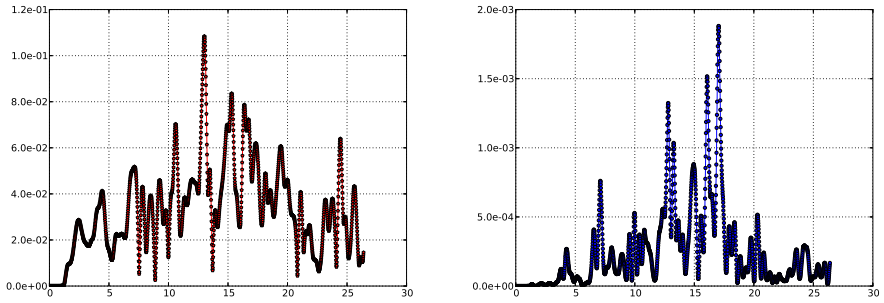

Figure 15: Evolution in time of the Euclidian norm of response (left) and energy rate (right) on the damaged zone.

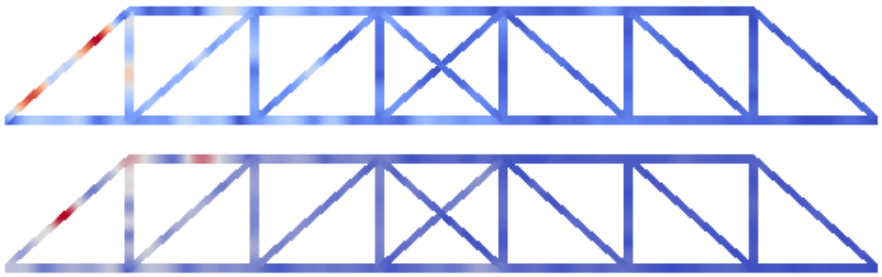

Figure 16: Euclidian norm as an image of the damage location for appropriate times selected from maximum value of energy (upper) and eulcidian (lower) norm evolutions. Sensors for recording considered on every s_i for $i \in [1,14]$.

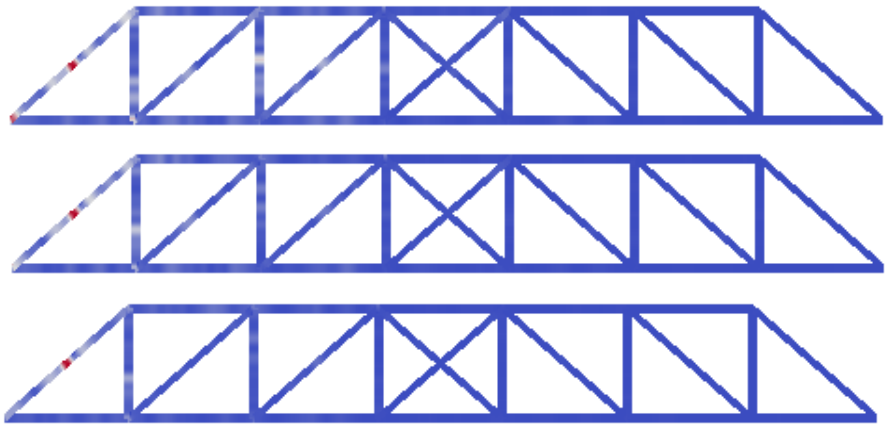

Figure 17: Energy density on appropriate time, selected from maximum value of energy evolution, as an image of the damage location for the three configurations of active sensors. Number of sensor is increased from upper to bottom pictures.

4 Imaging technique

Imaging is the discipline in science and engineering that consists of creating a representation of some medium, or structure, from recordings of waves that have propagated through (or scattered by) the medium. Imaging techniques, have a wide range of applications, e.g., optics, geophysics, medical, etc.. However, it seems that it is underestimated in the field of structural engineering. Here we try to define an imaging framework capable to deal with problems of structural systems and we, briefly, give an introduction for that matter, since it is an ongoing research topic of our group. The interested reader is referred to (Bleistein et al., 2001; Borcea et al., 2005) and references therein for further study.

4.1 Source localization

Here we use the time reversal process in order to define an imaging functional for the discrete system that we are interested in, similar to the procedure presented in (Tsogka et al., 2015) for the case of the continuous acoustic wave equation. Data at the receiver $u_r(t)$ and the solution of the backward problem at the i^{th} dof, $u_i^{TR}(t)$, might be given, using eq.(11), as:

$$u_r(t) = \int_0^t f_s(\tau) h_{rs}(t-\tau)\, d\tau, \tag{15}$$

$$u_i^{TR}(t) = \int_0^t u_r(T-\tau) h_{ri}(t-\tau)\, d\tau. \tag{16}$$

In practice we measure the data $u_r(t)$ physically or simulate it numerically. In the frequency domain, using Fourier transform we get

$$u_r(t) = \frac{1}{2\pi} \int_{-\infty}^{\infty} \widehat{h}_{rs}(\omega) \widehat{f}_s(\omega) \exp(i\omega t)\, d\omega, \quad \widehat{u}_r(\omega) = \widehat{h}_{rs}(\omega) \widehat{f}_s(\omega), \tag{17}$$

while the time reversed data in frequency domain is,

$$\widehat{u}_i^{TR}(\omega) = \widehat{h}_{ri}(\omega) \overline{\widehat{u}_r(\omega)} = \widehat{h}_{ri}(\omega) \overline{\widehat{h}_{rs}(\omega) \widehat{f}_s(\omega)} \tag{18}$$

where overline denotes complex conjugate. Therefore, in accordance also to eq. (13), the response obtained during the backward step for the i^{th} dof can be written as,

$$u_i^{TR}(t) = \frac{1}{2\pi} \int_{-\infty}^{\infty} \widehat{h}_{ri}(\omega) \overline{\widehat{h}_{rs}(\omega) \widehat{f}_s(\omega)} \exp(i\omega t)\, d\omega. \tag{19}$$

Recalling now that in time-reversal we send back the field recorded at all receivers r, see also eq. (14), we get the following expression for the time reversed field at the i^{th} dof,

$$u_i^{TR}(t) = \frac{1}{2\pi} \int_{-\infty}^{\infty} \sum_{r=1}^{N_r} \widehat{h}_{ri}(\omega) \overline{\widehat{h}_{rs}(\omega) \widehat{f}_s(\omega)} \exp(i\omega t)\, d\omega. \tag{20}$$

By evaluating the time-reversed field at time $t = 0$ which is the time at which we expect refocusing at the source we obtain

$$u_i^{TR}(t=0) = \frac{1}{2\pi} \int_{-\infty}^{\infty} \sum_{r=1}^{N_r} \widehat{h}_{ri}(\omega) \overline{\widehat{h}_{rs}(\omega) \widehat{f}_s(\omega)}\, d\omega. \tag{21}$$

This motivates us to define an imaging functional as

$$I_m = \frac{1}{2\pi} \sum_{\omega} \sum_{r=1}^{N_r} \overline{\widehat{h}_{rs}(\omega) \widehat{f}_s(\omega)} \widehat{h}_{rm}(\omega) = \frac{1}{2\pi} \sum_{\omega} \sum_{r=1}^{N_r} \overline{\widehat{u}_r(\omega)}\, \widehat{h}_{rm}(\omega) \tag{22}$$

which associates a value at the m^{th} dof by back propagating the recordings (data) reversed in time, $\overline{\widehat{u}_r(\omega)}$, using all receivers and all available frequencies.

4.2 Damage identification

Equivalently to the source localization process, in the present subsection we perform the backward step of the defect or damage localization problem in the frequency domain. For that purpose we consider the scattered field at the receivers, and based on existing models for the continuous medium (Borcea et al., 2005; Tsogka et al., 2015), we define an imaging functional, for the discrete system case, as

$$I_m = \sum_{\omega} \sum_{r=1}^{N_r} \overline{\widehat{u}^{\text{sc}}_{rs}(\omega)} \widehat{h}_{rm}(\omega) \widehat{h}_{rs}(\omega). \tag{23}$$

Here $\widehat{u}^{\text{sc}}_{rs}(\omega)$ is the scattered field recorded at dof r due to an excitation at dof s. If we have data for multiple excitations (sources) we superpose the images obtained for each one of them and obtain,

$$I_m = \sum_{\omega} \sum_{r=1}^{N_r} \sum_{s=1}^{N_s} \overline{\widehat{u}^{\text{sc}}_{rs}(\omega)} \widehat{h}_{rm}(\omega) \widehat{h}_{rs}(\omega). \tag{24}$$

We make clear at this point that I_m refers to the m^{th} dof of the system. One might want to construct an image using only a specific type of dof on each spatial location or we might consider images of quantities such as the energy that combine more than one dofs.

5 Conclusions

We presented in this chapter a methodology for localizing sources, as well as, small defects and/or damaged areas, found on frame structures that could be modeled by beam elements. Time reversal procedure and standard imaging techniques have been defined and presented. Numerical implementation for time reversal experiments have been formulated, using standard finite element approximations, by the adoption of the Timoshenko's beam theory and time integration algorithms. Some numerical examples have been solved and results have been indicatively demonstrated and proved to be very promising.

Acknowledgement
This work was partially supported by the European Research Council Starting Grant Project ADAPTIVES-239959.

References

Ammari, H., Bretin, E., Garnier, J., and Wahab, A. (2013). Time-reversal algorithms in viscoelastic media. *European Journal of Applied Mathematics*, 24(04):565–600.

Anderson, B. E., Griffa, M., Larmat, C., Ulrich, T. J., and Johnson, P. A. (2008). Time reversal. *Acoustics Today*, 4(1):5–16.

Bathe, K.-J. (2006). *Finite element procedures*. Klaus-Jurgen Bathe.

Bécache, E., Joly, P., and Tsogka, C. (2002). A new family of mixed finite elements for the linear elastodynamic problem. *SIAM Journal of Numerical Analysis*, 39:2109–2132.

Belytschko, T. and Hughes, T. J. (2014). Computational methods for transient analysis. *Computational Methods in Mechanics*, 1.

Bleistein, N., Cohen, J., and John, W. (2001). *Mathematics of multidimensional seismic imaging, migration, and inversion*. Springer Science+Business Media, New York.

Borcea, L., Papanicolaou, G., and Tsogka, C. (2005). Interferometric array imaging in clutter. *Inverse Problems*, 21(4):1419.

Clough, R. W. and Penzien, J. (1993). *Dynamics of structures*. McGraw-Hill, Singapore.

Cook, R. D., Malkus, D. S., Plesha, M. E., and Witt, R. J. (2001). *Concepts and application of finite element analysis*. John Wiley & sons, inc., United States, fourth edition.

Cowper, G. R. (1966). The shear coefficient in Timoshenko's beam theory. *Journal of Applied Mechanics*, 33:335–340.

Doyle, J. F. (1989). *Wave Propagation in Structures: An FFT-Based Spectral Analysis Methodology*. Springer-Verlag, New York.

Fink, M., Cassereau, D., Derode, A., Prada, C., Roux, P., Tanter, M., Thomas, J.-L., and Wu, F. (2000). Time-reversed acoustics. *Reports on progress in Physics*, 63(12):1933.

Fink, M. and Prada, C. (2001). Acoustic time-reversal mirrors. *Inverse problems*, 17(1):R1.

Fung, Y. C. (1965). *Foundations of solids mechanics*. Prentice-Hall, Englewood Cliffs, New Jersey.

Givoli, D. (2014). Time reversal as a computational tool in acoustics and elastodynamics. *Journal of Computational Acoustics*, 22(03).

Gopalakrishnan, S., Chakraborty, A., and Mahapatra, D. R. (2008). *Spectral finite element method: Wave propagation, diagnostics and control in anisotropic and inhomogeneous structures*. Springer, London.

Graff, K. F. (1975). *Wave Motion in Elastic Solids*. Dover publications, New York.

Guennec, Y. L., Savin, E., and Clouteau, D. (2013). A time-reversal process for beam trusses subjected to impulse loads. *Journal of Physics: Conference Series*, 464(012001).

Hartmann, F. (2013). *Green's functions and finite elements*. Springer, Berlin Heidelberg.

Kohler, M. D., Heaton, T. H., and Heckman, V. (2009). A time-reversed reciprocal method for detecting high-frequency events in civil structures with accelerometer arrays. In *Proc. of the 5th International Workshop on Advanced Smart Materials and Smart Structures Technology*.

Le Guennec, Y. and Savin, É. (2011). A transport model and numerical simulation of the high-frequency dynamics of three-dimensional beam trusses. *The Journal of the Acoustical Society of America*, 130(6):3706–3722.

Panagiotopoulos, C. G., Paraskevopoulos, E. A., and Manolis, G. D. (2011). Critical assessment of penalty-type methods for imposition of time-dependent boundary conditions in fem formulations for elastodynamics. In *Computational Methods in Earthquake Engineering*, pages 357–375. Springer.

Panagiotopoulos, C. G., Petromichelakis, Y., and Tsogka, C. (2015). Time reversal in elastodynamics with application to structural health monitoring. In *Proc. of the 5th International Conference on Computational Methods in Structural Dynamics and Earthquake Engineering*.

Paraskevopoulos, E., Panagiotopoulos, C., and Manolis, G. (2010). Imposition of time-dependent boundary conditions in fem formulations for elastodynamics: critical assessment of penalty-type methods. *Computational Mechanics*, 45:157–166.

Prada, C., Thomas, J.-L., and Fink, M. (1995). The iterative time reversal process: Analysis of the convergence. *The Journal of the Acoustical Society of America*, 97(1):62–71.

Przemieniecki, J. (1968). *Theory of matrix structural analysis*. Dover publications, inc., New York.

Simo, J. and Tarnow, N. (1992). The discrete energy-momentum method. conserving algorithms for nonlinear elastodynamics. *Journal of Applied Mathematics and Physics*, 43:757–792.

Timoshenko, S. P. (1921). On the correction for shear of the differential equation for transverse vibrations of bars of uniform cross-section. *Philosophical Magazine*, 41:744–746.

Timoshenko, S. P. (1922). On the transverse vibrations of bars of uniform cross-section. *Philosophical Magazine*, 43:125–131.

Tsogka, C., Petromichelakis, Y., and Panagiotopoulos, C. G. (2015). Influence of the boundaries in imaging for damage localization in 1d domains. In *Proc. of the 8th GRACM International Congress. on Computational Mechanics*.

Yavuz, M. E. and Teixeira, F. L. (2009). Ultrawideband microwave sensing and imaging using time-reversal techniques: A review. *Remote Sensing*, 1(3):466–495.